Supporting Information

Tight bonding and high-efficiency utilization of S-S moieties to enable ultra-stable and high-capacity alkali-metal conversion batteries

Keyi Chen,[abc] *Wujie Qiu,*[ab] *Qingping Wu,*[ac] *Xuejun Zhou,*[abc] *Jianjun Liu*[ab] *and Chilin Li* *[abc]

[a] State Key Laboratory of High Performance Ceramics and Superfine Microstructure, Shanghai Institute of Ceramics, Chinese Academy of Sciences, 585 He Shuo Road, Shanghai 201899, China. Email: chilinli@mail.sic.ac.cn

[b] Center of Materials Science and Optoelectronics Engineering, University of Chinese Academy of Sciences, Beijing 100049, China.

[c] CAS Key Laboratory of Materials for Energy Conversion, Shanghai Institute of Ceramics, Chinese Academy of Sciences, Shanghai 201899, China.

Experimental Section

Synthesis of Pyrite Samples. Before the preparation of FeS_2@S and FeS_2 samples, the corresponding iron-based fluoride precursors of FeF_2 and FeF_3 were respectively decorated via a simple polydopamine (PDA) coating method.[S1] In a typical synthesis, the commercial FeF_2 (Alfa Aesar, 98%) or FeF_3 (Strem, 99%) powder and dopamine hydrochloride (Aladdin, 98%) in a mass ratio of 2:1 were successively dispersed into Tris-buffer solution (10 mM, pH ≈ 8.5) with magnetic stirring for 12 h. The resultant product was collected via centrifugation, washed with deionized water and ethanol, followed by subsequent drying under vacuum at 80 ℃ overnight. The sulfuration process refers to our previous work.[S2] In brief, the FeF_2-PDA (or

FeF_3-PDA) and elemental sulfur (Sigma Aldrich, 99.995%) were mixed in a molar ratio of 6:7 (or 4:5) and continuously heated at 500 ℃ with a rising rate of 2 ℃/min for 10 h under evacuated and sealed condition. The excess sulfur probably precipitates in the final product.

Synthesis of Carbon Derivative from FeF_x-PDA. For preparation of the carbon derivative FeF_x-PDA-C, the PDA-coated fluorides were annealed without simultaneous sulfuration, and they transform into Fe-FeC_x@C composites. The annealed products were etched in concentrated HCl solution for 10 h to remove Fe-contained species. Finally, the resulting carbon derivatives were obtained by washing with deionized water, filtrating and drying under vacuum overnight.

Visualized Polysulfide Adsorption Test. Li_2S_4 solution (0.25 M) was prepared by dissolving sulfur and lithium sulfide (Li_2S) with a molar ratio of 3:1 in tetraethylene glycol dimethyl ether (TEGDME, Sigma Aldrich) followed by vigorous magnetic stirring for 24 h at 60 ℃. The concentration of solution was further diluted into 2.5 mM for adsorption test. 10 mg FeF_2-PDA-C, FeF_3-PDA-C or 20 mg commercial FeS_2 were dispersed in 4.0 mL of the diluted Li_2S_4/TEGDME solution to achieve thorough adsorption by stirring for 10 h. After adsorption, the suspensions were stayed for a long time until the absorbents were completely precipitated with clear supernatant solutions, for a comparison with the blank control of diluted Li_2S_4 solution.

Physical Characterization. The components and crystallographic structure of both the pyrite samples were analyzed by X-ray powder diffractometer (XRD, Bruker, D8 Discover) with Cu Kα radiation in a 2θ range of 10 °–80 ° at a scan rate of 5 °/min. The scanning electron microscopy (SEM, Magellan 400L, FEI) equipped with energy dispersive X-ray spectroscope (EDS) were carried out to observe the morphology, grain size, and element distribution. Transmission electron microscopy (TEM) images and selected area electron diffraction (SAED) patterns of FeS_2@S were collected on JEOL JSM-6700F operated at an acceleration voltage of 200 kV to further confirm the morphology, microstructure, and phase assignment. X-ray photoelectron spectra (XPS) were obtained by PHI5300 XPS spectrometer (250W, 14kV) with an Mg anode source to detect the surface component, elemental valence, and bonding situation of FeS_2@S

and FeS_2. DSC 800 from PerkinElmer was performed to take the thermogravimetric analysis (TGA) results under N_2 gas stream and the heating rate of 10 ℃/min.

Electrochemical Measurement. To preparing the cathodes, a mixture of pyrite powder (FeS_2@S or FeS_2), super P and poly (vinyl difluoride) (PVDF, which is uniformly dissolved in 1-methyl-2-pyrrolidinone NMP) with a weight ratio of 7:2:1 was pasted on pure copper foil and dried in vacuum at 50 ℃ for 20 h to remove solvent. CR2032-type coin cells were assembled with pyrite cathode, high-purity Li/Na metal anode and glass fiber separator (GF/B, Whatman) in an Ar-filled glove box (<0.1 ppm for water and oxygen). The electrolyte solution for Li or Na metal batteries was prepared by dissolving 1M lithium bis(trifluoromethane)sulfonamide (LiTFSI, Sigma Aldrich) or 1 M sodium trifluomethanesulfonate ($NaSO_3CF_3$, Aladdin) in diglyme (DGM, Sigma Aldrich, 99.5%), respectively. Galvanostatic charge-discharge measurements of pyrite cathodes vs. Li/Li^+ (Na/Na^+) were performed at room temperature under different rates from 0.1 to 10 C in a voltage range of 1.0−3.0 V for Li cells or 0.5−3.0 V for Na cells on the Land multichannel battery testing system (CT2001A). One C denotes the current density to theoretically achieve four-electron transfer within 1 h for FeS_2. Impedance measurements of cells based on different pyrites before cycling and after different cycling at 1C were done by using a Solartron frequency analyzer (1260−1296) in a frequency range from 100 kHz to 0.1 Hz. Cyclic voltammetry (CV) and Tafel analysis were carried out on an electrochemical workstation (VersaSTAT3, AMETEK Scientific Instruments). CV measurements were run in a voltage range from 1.0 to 3.0 V for Li cells or from 0.5 to 3.0 V for Na cells at different scan rates from 0.2 to 1.5 mV/s. Tafel analysis was performed on the tenth discharge process by holding the Li or Na cells at 1.62 V or 1.52 V respectively (i.e. at the voltage of dominant conversion plateau) for 1 h, followed by a linear scan at 1 mV/s in the voltage range of ±150 mV around the open-circuit voltage.

Calculation Details. The first-principles calculations were performed in the framework of the density-function theory using the plane wave basis VASP code,[S3,S4] implementing the generalized gradient approximation (GGA) of

Perdew-Burke-Ernzerhof (PBE) form.[S5] The interactions between the ions and electrons were described by the all-electron projector augmented wave (PAW) method,[S6,S7] with plane waves up to a cutoff energy of 500 eV. The Hubbard U (DFT+U) correction was used, and an effective interaction parameter U_{eff} = 5.3 eV was used for Fe 3d electrons.[S8] Spin polarized calculations were performed in all configurations. To avoid the interactions between adjacent layers, the vacuum distance was set to 20 Å. The Brillouin-zone integrations were performed on the grid of Monkhorst-Pack procedure with 2×2×1 k-point meshes.[S9] The binding strength between S_8/Li_2S_n and the substrate material (SM) was evaluated by the binding energy (E_b), which is described as $E_b = E_{S_8/Li_2S_n+SM} - E_{S_8/Li_2S_n} - E_{SM}$, where E_{SM}, E_{S_8/Li_2S_n} and E_{S_8/Li_2S_n+SM} represent the total energies of the substrate, the sulfur molecule S_8 (or polysulfide molecule Li_2S_n), and the pair of substrate and sulfur molecule S_8 (or polysulfide molecule Li_2S_n). Therefore, a negative binding energy shows that the binding interaction between S_8/Li_2S_n and SM is favored.

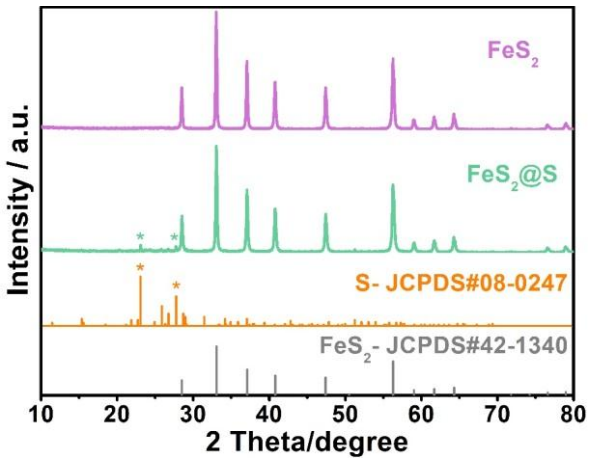

Figure S1. XRD patterns of FeS_2 and FeS_2@S in a 2θ range of 10°–80°.

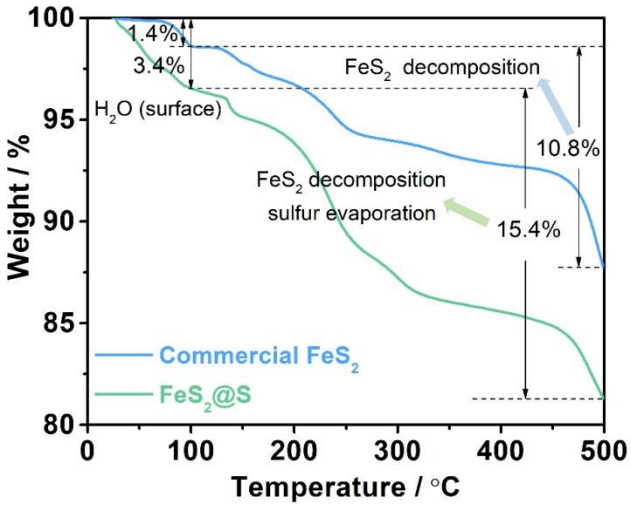

Figure S2. TGA curves of FeS_2@S and commercial FeS_2 with weight loss estimated based on the mass evolution under an N_2 gas steam from room temperature to 500 ℃. Nanostructured FeS_2@S tends to absorb moisture during air exposure, thus more weight loss below 120 ℃ corresponds to the removal of surface water. At higher temperatures, pyrite probably undergoes partial decomposition involving the escape of S-S moieties from FeS_2 lattices under N_2 flowing.[S10] More dramatic TGA curve dropping for FeS_2@S within a temperature range of 100–500 ℃ is associated with the complete evaporation of elemental sulfur.

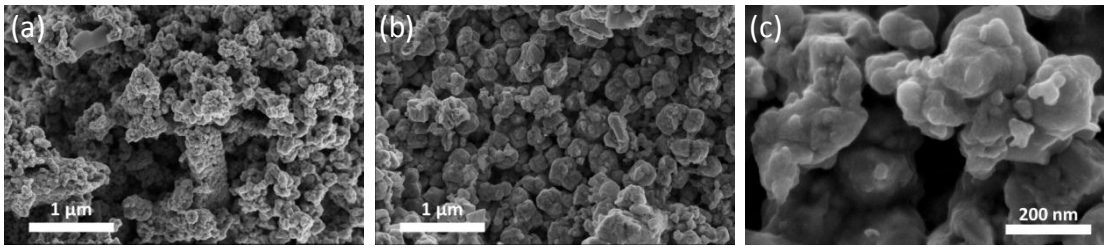

Figure S3. SEM images of (a) FeS_2@S and (b) FeS_2 in overview scale. (c) SEM image of FeS_2 in magnified scale.

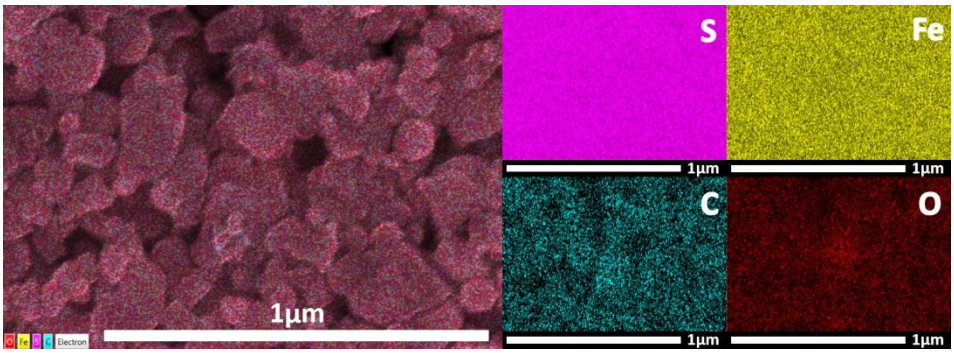

Figure S4. EDS mapping images (containing Fe, S, C and O elements) of FeS_2@S.

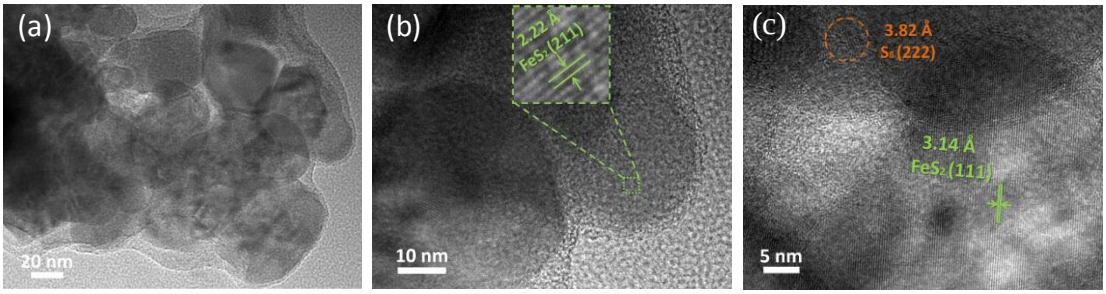

Figure S5. (a) TEM and (b,c) HRTEM images of FeS_2@S. Continuous and conformal carbon coatings on the surface of compactly stacked grains are clearly observed. The typical stripes with lattice d-spacing of 2.22 Å and 3.14 Å correspond to (211) and (111) planes of cubic FeS_2 phase. The S lattice stripes for (222) plane are found in the grain boundary.

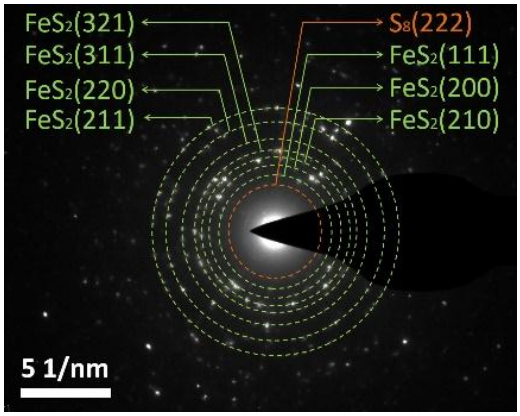

Figure S6. SAED pattern of FeS_2@S. There is a vague diffraction ring with small radius, which is assigned to (222) plane of elemental sulfur, besides the dominant diffraction rings belonging to pyrite FeS_2 phase.

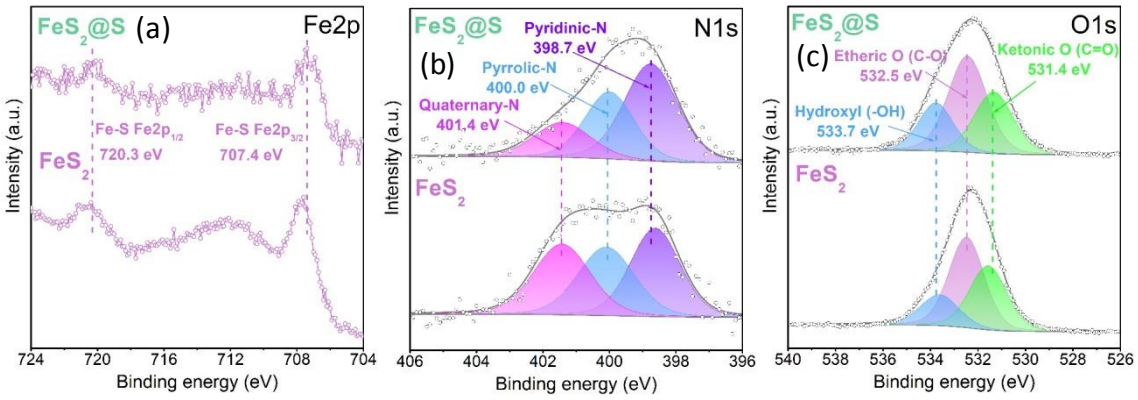

Figure S7. XPS spectra of (a) Fe 2p, (b) N 1s and (c) O 1s for FeS_2@S and FeS_2.

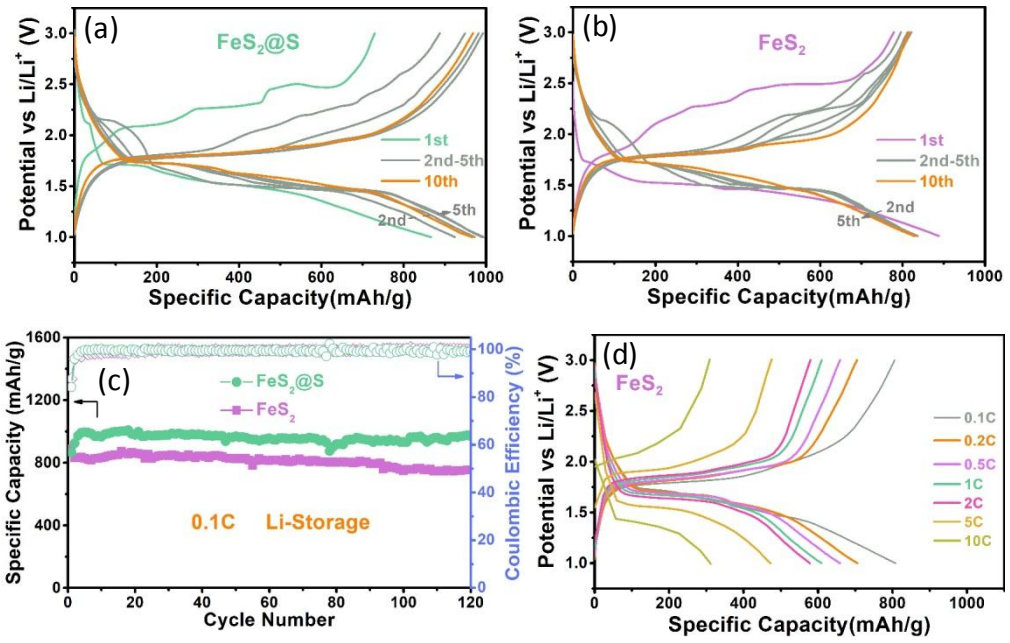

Figure S8. Galvanostatic charge-discharge curves of Li cells based on (a) FeS_2@S and (b) FeS_2 cathodes during the first ten cycles at 0.1 C in a voltage range of 1.0–3.0 V. (c) Cycling performance and coulombic efficiency of FeS_2@S and its comparison with FeS_2 at 0.1 C. (d) Galvanostatic charge-discharge curves of Li/FeS_2 cell depending on various rates from 0.1 to 10 C. The capacity of Li/FeS_2@S cell undergoes an activation process and even exceeds the theoretical value of pyrite during initial cycles, indicating an effective utilization of extra S–S moieties.

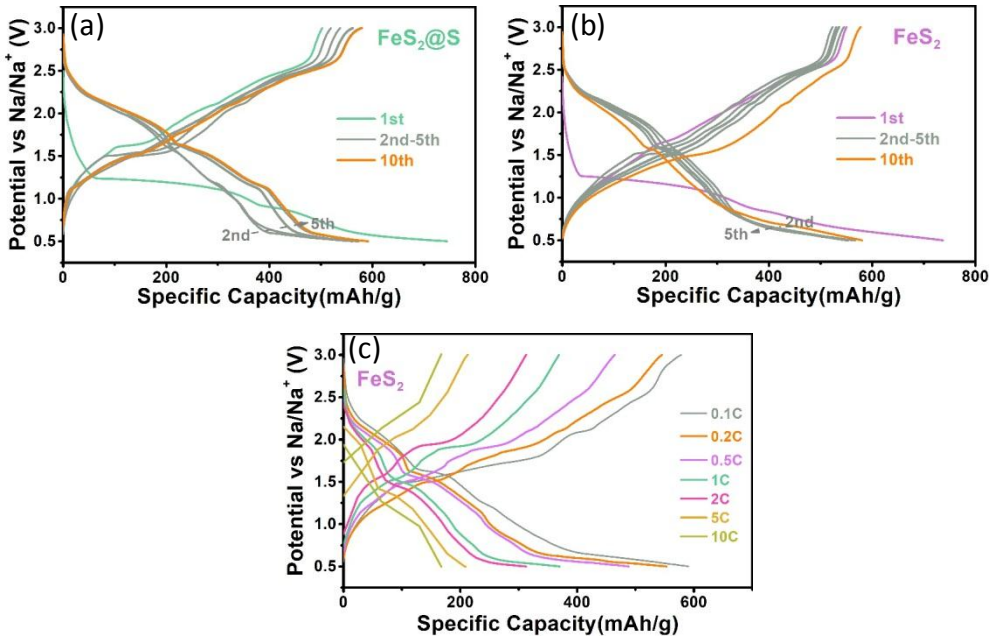

Figure S9. Galvanostatic charge-discharge curves of Na cells based on (a) FeS_2@S and (b) FeS_2 cathodes in a voltage range of 0.5–3.0 V at 0.2 C during the first ten cycles. (c) Galvanostatic charge-discharge curves of Na/FeS_2 cell under different rates from 0.1 to 10 C.

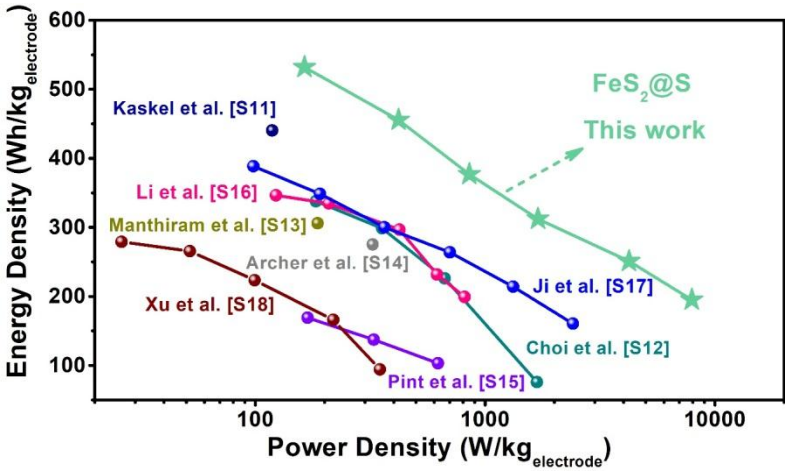

Figure S10. Comparison of energy and power densities between Na/FeS_2@S cell and some reported room temperature Na–S batteries. The energy/power density is estimated based on the weight of electrode including active material, conductive additive and binder.

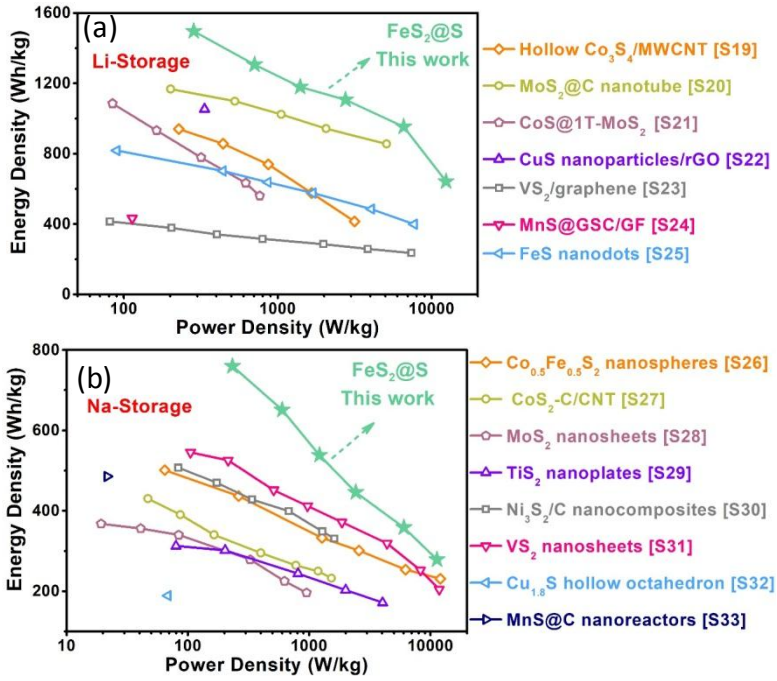

Figure S11. Ragone plots of as-prepared FeS_2@S composite and other typical metal sulfides for (a) Li-storage and (b) Na-storage.

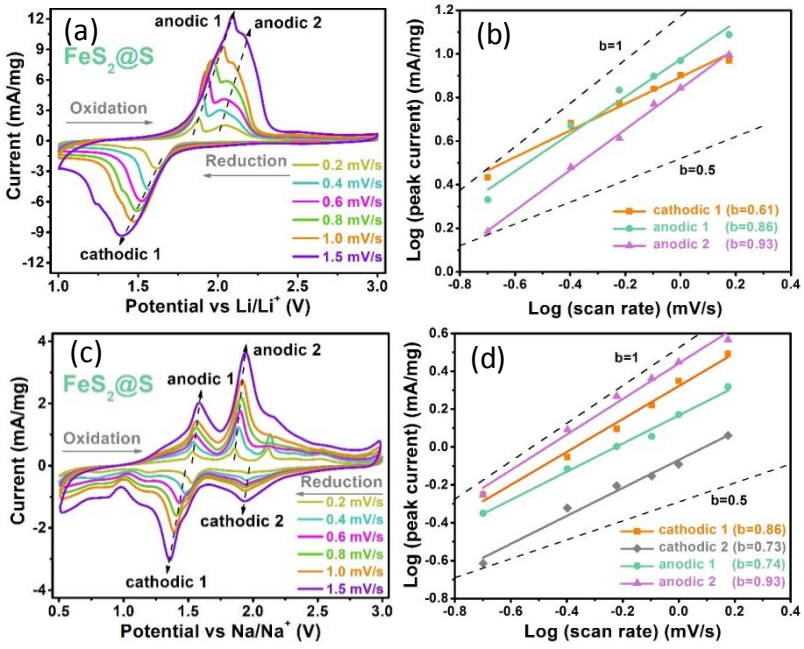

Figure S12. CV curves of FeS_2@S cathode at various scan rates from 0.2 to 1.5 mV/s (a) between 1.0 and 3.0 V for Li cell and (c) between 0.5 and 3.0 V for Na cell with the characteristic peaks labeled. Power law dependence of measured current on scan rate at the positions of characteristic peaks in CV curves based on $\log i(V) = b \log v + \log a$ for (b) Li cell and (d) Na cell based on FeS_2@S cathode.

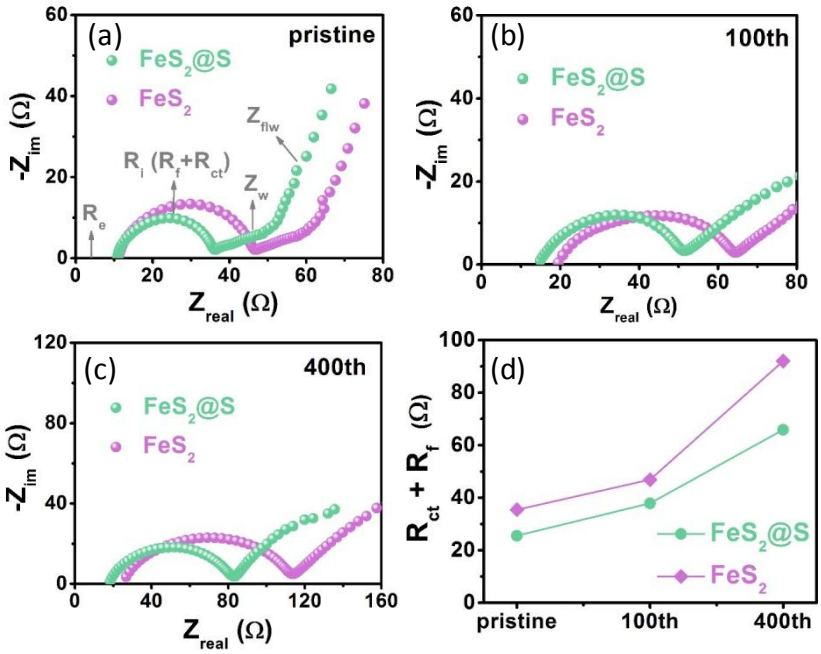

Figure S13. Electrochemical impedance spectra of (a) pristine and cycled Li cells based on FeS_2@S and FeS_2 cathodes after (b)100 cycles and (c) 400 cycles at 1 C. (d) Corresponding evolution of interface resistance R_i values (from the total contribution of SEI resistance R_f and charge transfer resistance R_{ct}) for pristine and cycled Li cells.

Table S1. Computational details of binding energies between Li_2S_n species and FeS_2 substrate. The energies of FeS_2, Li_2S_n molecules, their combinations, and corresponding binding energies are tabulated.

Polysulfide Molecules	E_{Li2Sn} (eV)	Substrate	E_{SM} (eV)	$E_{Li2Sn+SM}$ (eV)	E_b (eV)
Li_2S	-7.91			-685.23	-2.59
Li_2S_2	-13.02			-688.98	-1.23
Li_2S_4	-22.38	FeS_2	-674.73	-701.69	-4.58
Li_2S_6	-32.40			-710.57	-3.44
Li_2S_8	-39.13			-711.79	2.07

References

[S1] M. H. Ryou, Y. M. Lee, J. K. Park, J. W. Choi, *Adv. Mater.* **2011**, *23*, 3066.

[S2] K. Y. Chen, Y. Zhang, C. L. Li, *ACS Nano* **2018**, *12*, 12444.

[S3] G. Kresse, J. Furthmüller, *Comp. Mater. Sci.* **1996**, *6*, *15*.

[S4] G. Kresse, J. Furthmüller, *Phys. Rev. B* **1996**, *54*, 11169.

[S5] J. P. Perdew, K. Burke, M. Ernzerhof, *Phys. Rev. Lett*. **1996**, *77*, 3865.

[S6] P. E. Blöchl, *Phys. Rev. B* **1994**, *50*, 17953.

[S7] G. Kresse, D. Joubert, *Phys. Rev. B* **1999**, *59*, 1758.

[S8] A. Jain, S. P. Ong, G. Hautier, W. Chen, W. D. Richards, S. Dacek, S. Cholia, D. Gunter, D. Skinner, G. Ceder, *APL Mater.* **2013**, *1*, 011002.

[S9] H. J. Monkhorst, J. D. Pack, *Phys. Rev. B* **1976**, *13*, 5188.

[S10] S. Dallek, B. Larrick, *Thermochim. Acta* **1985**, *95*, 139.

[S11] M. Kohl, F. Borrmann, H. Althues, S. Kaskel, *Adv. Energy Mater.* **2016**, *6*, 1502185.

[S12] T. H. Hwang, D. S. Jung, J. S. Kim, B. G. Kim, J. W. Choi, *Nano Lett*. **2013**, *13*, 4532.

[S13] X. W. Yu, A. Manthiram, *Adv. Energy Mater.* **2015**, *5*, 1500350.

[S14] S. Y. Wei, S. M. Xu, A. Agrawral, S. Choudhury, Y. Y. Lu, Z. Y. Tu, L. Ma, L. A. Archer, *Nat. Commun*. **2016**, *7*, 11722.

[S15] R. Carter, L. Oakes, A. Douglas, N. Muralidharan, A. P. Cohn, C. L. Pint, *Nano*

Lett. **2017**, *17*, 1863.

[S16] C. L. Wang, H. Wang, X. F. Hu, E. Matios, J. M. Luo, Y. W. Zhang, X. Lu, W. Y. Li, *Adv. Energy Mater.* **2018**, *9*, 1803251.

[S17] T. J. Wu, M. J. Jing, L. Yang, G. Q. Zou, H. S. Hou, Y. Zhang, Y. Zhang, X. Y. Cao, X. B. Ji, *Adv. Energy Mater.* **2019**, *9*, 1803478.

[S18] T. T. Yang, W. Gao, B. S. Guo, R. M. Zhan, Q. J. Xu, H. He, S. J. Bao, X. Y. Li, Y. M. Chen, M. W. Xu, *J. Mater. Chem. A* **2019**, *7*, 150.

[S19] R. Tian, Y. Zhou, H. N. Duan, Y. P. Guo, H. Li, K. F. Chen, D. F. Xue, H. Z. Liu, *ACS Appl. Energy Mater.* **2018**, *1*, 402.

[S20] X. Q. Zhang, X. N. Li, J. W. Liang, Y. C. Zhu, Y. T. Qian, *Small* **2016**, *12*, 2484.

[S21] J. Lu, G. L. Xia, S. P. Gong, C. L. Wang, P. Jiang, Z. Y. Lin, D. D. Wang, Y. Yang, Q. W. Chen, *J. Mater. Chem. A* **2018**, *6*, 12613.

[S22] X. D. Ding, S. Lei, C. F. Du, Z. L. Xie, J. R. Li, X. Y. Huang, *Adv. Mater. Interfaces* **2019**, *6*, 1900038.

[S23] W. Y. Fang, H. B. Zhao, Y. P. Xie, J. H. Fang, J. Q. Xu, Z. W. Chen, *ACS Appl. Mater. Interfaces* **2015**, *7*, 13044.

[S24] X. Gao, B. Y. Wang, Y. Zhang, H. Liu, H. K. Liu, H. Wu, S. X. Dou, *Energy Storage Mater.* **2019**, *16*, 46.

[S25] C. B. Zhu, Y. R. Wen, P. A. van Aken, J. Maier, Y. Yu, *Adv. Funct. Mater.* **2015**, *25*, 2335.

[S26] K. Zhang, M. Park, L. M. Zhou, G. H. Lee, J. Shin, Z. Hu, S. L. Chou, J. Chen, Y. M. Kang, *Angew. Chem. Int. Ed.* **2016**, *55*, 12822.

[S27] Y. Ma, Y. J. Ma, D. Bresser, Y. C. Ji, D. Geiger, U. Kaiser, C. Streb, A. Varzi, S. Passerini, *ACS Nano* **2018**, *12*, 7220.

[S28] X. Q. Xie, T. Makaryan, M. Q. Zhao, K. L. Van Aken, Y. Gogotsi, G. X. Wang, *Adv. Energy Mater.* **2016**, *6*, 1502161.

[S29] Y. P. Liu, H. T. Wang, L. Cheng, N. Han, F. P. Zhao, P. R. Li, C. H. Jin, Y. G. Li, *Nano Energy* **2016**, *20*, 168.

[S30] X. Zhao, H. E. Wang, R. C. Massé, J. Cao, J. H. Sui, J. Y. Li, W. Cai, G. Z. Cao, *J. Mater. Chem. A* **2017**, *5*, 7394.

[S31] D. X. Yu, Q. Pang, Y. Gao, Y. J. Wei, C. Z. Wang, G. Chen, F. Du, *Energy Storage Mater.* **2018**, *11*, 1.

[S32] H. Park, J. Kwon, H. Choi, D. Shin, T. Song, X. W. Lou, *ACS Nano* **2018**, *12*, 2827.

[S33] Y. N. Liu, L. P. Li, J. H. Zhu, T. Meng, L. Ma, H. Zhang, M. W. Xu, J. Jiang, C. M. Li, *ACS Appl. Mater. Interfaces* **2018**, *10*, 27911.